

Integration of a Traveling-Wave Electro-Absorption Modulator with a Widely Tunable SG-DBR Laser

Matthew M. Dummer¹, *Student Member, IEEE*, Matthew N. Sysak¹, *Student Member, IEEE*,
James W. Raring², *Member, IEEE*, Anna Tauke-Pedretti¹, *Student Member, IEEE*,
and Larry A. Coldren¹, *Fellow, IEEE*

¹University of California Santa Barbara, ECE Department, Santa Barbara, CA 93106 USA
dummer@engineering.ucsb.edu

² Sandia National Laboratories, Albuquerque, NM 87185 USA

Abstract

A widely tunable transmitter integrating a sampled grating DBR laser and traveling wave EAM with on-chip termination is presented. The transmitter exhibits a 23 GHz bandwidth, greater than 1 mW output power, and wavelength tuning over 30 nm.

I. INTRODUCTION

TRAVELING wave electro-absorption modulators (TW-EAMs) are attractive solutions for high-bandwidth optical modulators in InP. These types of modulators are advantageous due to their small footprint, low drive voltage, and high speed operation. Although many discrete TW-EAMs have been reported [1]–[5] exhibiting 3-dB bandwidths as high as 90 GHz, very few devices have been integrated with semiconductor lasers [6]. In this work we demonstrate the first widely tunable transmitter based on a traveling wave electro-absorption modulator (TW-EAM) integrated with a sampled grating DBR (SG-DBR) laser. The EAM is designed with a transmission line electrode and integrated impedance matched termination, such that the response exceeds the RC time constant limitation of traditional lumped element devices. The 3-dB bandwidth is greater than 23 GHz and the frequency response roll-off is improved by 10 dB/decade due to traveling wave effects. The transmitter is capable of high output powers (>2 mW) with extinction ratios ranging from 8 to 12 dB for wavelengths between 1524 and 1555 nm at data rates of 10 Gbps.

II. DESIGN AND FABRICATION

The transmitter consists of a five stage SG-DBR laser followed by an output semiconductor optical amplifier (SOA) and TW-EAM shown in Fig. 1. The device was fabricated using a dual quantum well (DQW) base structure similar to that in [7]. A diagram of the epitaxial layer structure is shown in Fig. 2. A quantum well (QW) stack grown above the waveguide with a photo luminescence peak (λ_{PL}) of 1540 nm provides the gain for laser and SOA. These upper QWs are selectively removed from all regions of the device except the 500 μm long laser gain section and 400 μm long SOA before the p-type cladding is grown. A second set of QWs centered in the waveguide provide modulation efficiency by utilizing the quantum confined stark effect (QCSE). However, the centered wells are detuned ($\lambda_{PL} = 1455$ nm) from the lasing wavelength to maintain low passive waveguide loss under no

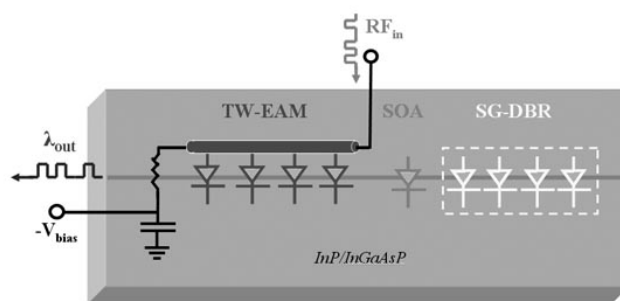


Fig. 1. Circuit diagram of fabricated TW-EAM transmitter with integrated load resistor and capacitor

applied bias. The TW-EAM was designed with microstrip line geometry such that the electrical signal propagates in the same direction as the optical signal along the 400 μm long modulator ridge. The ridge of the TW-EAM is 2.5 μm wide supported on a 6 μm wide deeply etched mesa to reduce capacitance and allow for the incorporation of a AuGe ground plane close to the ridge for low RF loss. The ground plane and ridge are buried in a photo-defined benzocyclobutene (BCB) as a low-k dielectric. The microstrip electrode contacts the ridge through a via in the BCB as depicted in the schematic cross section in Fig. 3. High speed pads on the input side of the modulator allow for wirebonding or directly driving the TW-EAM with a signal-ground (SG) probe. The electrode is terminated by an impedance matched thin-film NiCr resistor deposited by electron-beam evaporation. In series with the resistor is a 30 pF on-chip capacitor formed by sandwiching 250 nm of silicon nitride between a top Au plate and the AuGe ground plane. The capacitor is designed to eliminate DC power dissipation in the resistor while still providing an effective RF ground path. Additionally, the on-chip capacitor is wire bonded to a larger capacitor (220 nF) mounted on the carrier in parallel to improve the low frequency response. This is especially important for achieving low pattern dependence

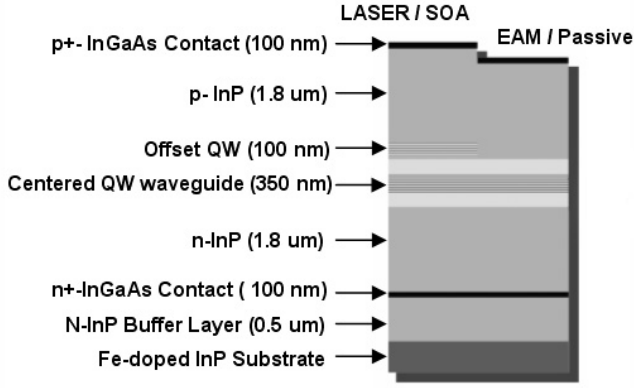


Fig. 2. Epitaxial layer structure for dual quantum well TW-EAM transmitter.

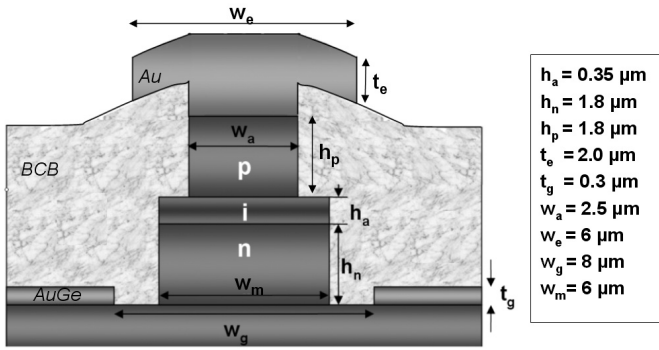


Fig. 3. Schematic cross section and dimensions of fabricated TW-EAM.

during transmission of digital data with long word lengths.

III. TRAVELING WAVE EXPERIMENTS

Two-port electrical S-parameter measurements have been performed on the TW-EAM to determine its transmission line behavior. The characteristic impedance, electrical effective index, and microwave loss versus frequency were determined using the ABCD method described in [8] and are shown in Fig. 4 & 5. The characteristic impedance (Z_0) is 22Ω and the electrical index is about 6.5 demonstrating a 62% mismatch between the optical and electrical traveling waves. These values are typical of such capacitively loaded microstrip lines and we have observed good agreement with simulations using the method described in [9] based on the device geometry. The microwave loss is highly frequency dependant and increases as $0.55 \text{ cm}^{-1}/\text{GHz}$ (or $0.24 \text{ dB}/(\text{mm} \cdot \text{GHz})$). Measurements of both loaded and unloaded transmission lines show that over 80% of this loss is due to the series resistance of the reverse biased TW-EAM diode. The remainder can be attributed to the microwave losses of the metal electrode at high frequencies.

Due to the integration of the laser and electrical terminations on this device, it is not possible to directly measure the traveling wave benefit in the frequency response. Instead, discrete TW-EAMs were fabricated on the same wafer so that light could be coupled in from either facet to compare the co- and counter-propagating electrical-to-optical (EO) response.

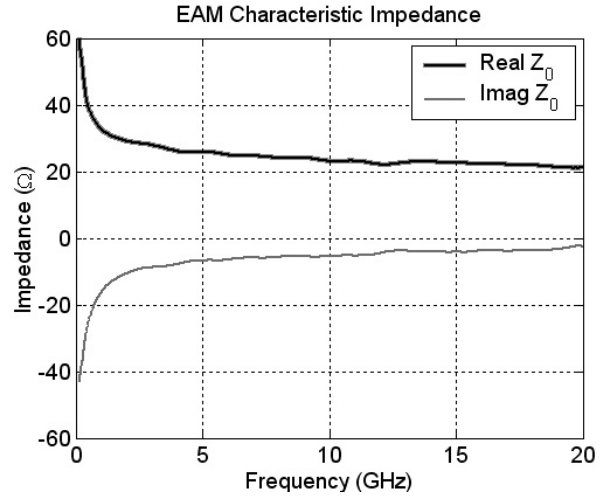


Fig. 4. Characteristic impedance (Z_0) vs. frequency of TW-EAM extracted from two-port S-parameters. The DC bias was -2 V.

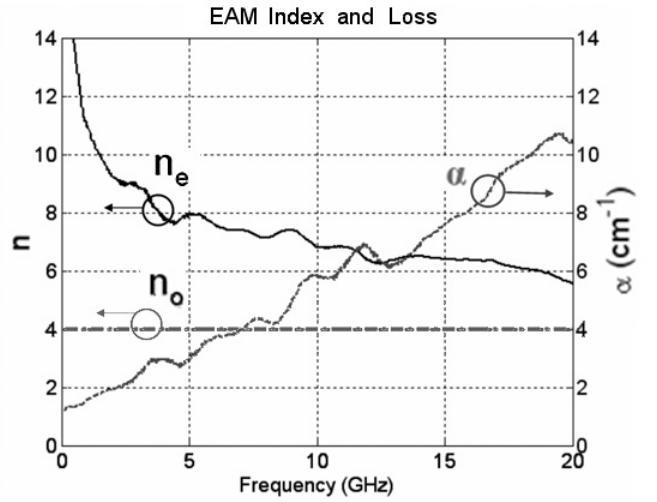


Fig. 5. Electrical effective index (n_e) compared with optical group index (n_o) and microwave loss coefficient (α).

The integrated resistor value used for this experiment was 20Ω to be matched to Z_0 of the TW-EAM. The small signal frequency responses for the modulator are shown in Fig. 5. The response of the co-propagating measurement has a 3-dB bandwidth of 23 GHz and rolls off by 10 dB/decade compared to 20 GHz and 20 dB/decade when the optical and electrical signals travel in opposite directions.

IV. TRANSMITTER PERFORMANCE

The SG-DBR with post-amplifier is capable of producing up to 10 dBm of fiber coupled output power over the continuous tuning range of 1524 nm to 1565 nm (Fig. 8). The TW-EAM efficiency has been measured over the tuning range of SG-DBR laser. Figure 7 shows the measured DC extinction characteristics of the integrated modulator. The extinction curve is highly dependent on the lasing wavelength and shows significant improvement in efficiency as the detuning from the centered QW band edge is reduced. The maximum slope

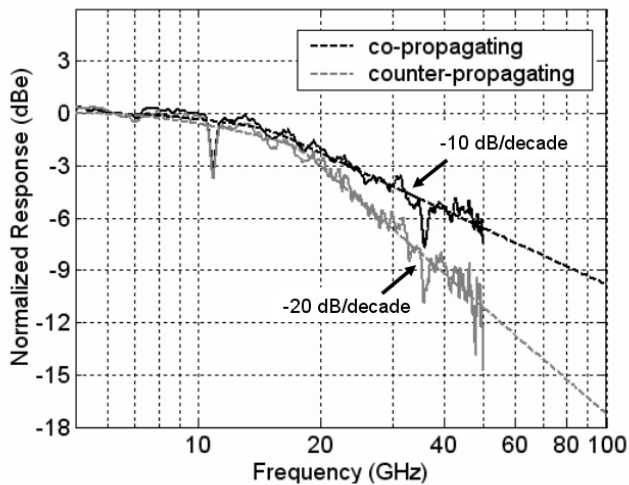


Fig. 6. Small signal EO measurement comparing co- and counter-propagating traveling wave response for -1.5 V bias.

efficiency ranges from 10 dB/V for 1559 nm to as high as 25 dB/V for 1522 nm.

Transmission of digital data has been performed at 10 Gbps non-return to zero (NRZ). DC bias currents for the laser and SOA were 120 mA and 100 mA, respectively. The modulator was directly driven using a SG coplanar probe and biased across the on-chip capacitor as shown in Fig 1. An on-chip termination resistance of 35Ω was used to reduce the mismatch between the EAM and the 50Ω electrical driver circuit. Open eye diagrams were observed over a 30 nm range of wavelengths and are shown in Fig. 8. The TW-EAM DC bias for the 1524 nm, 1539 nm, and 1555 nm transmission were -2.1 V, -2.7 V, and -3.5 V to take advantage of the steepest part of the modulator extinction curves for each respective wavelength. Extinction ratios (E.R.) as high as 12 dB and eye amplitudes (P_{out}) as high as 2 mW, fiber coupled, were achieved for an electrical drive voltage of 2 V peak-to-peak.

V. CONCLUSION

We have demonstrated a traveling wave electro-absorption modulator based transmitter tunable over 30 nm. The device includes an integrated matched electrical termination to simplify biasing and reduce microwave loss. The TW-EAM design exhibits a 2x improvement in the response slope due to the traveling wave enhancement. Transmission of digital data at 10 Gbps NRZ has been achieved with greater than 8 dB extinction and 1 mW output power over the laser tuning range. Future work will focus on improving device performance to accommodate much higher data rates. This will be accomplished by raising the characteristic impedance of the TW-EAM to reduce the mismatch and improve the series resistance for lower microwave loss.

REFERENCES

[1] T. Yamanaka, K. Tsuzuki, N. Kikuchi, E. Yamada, Y. Shibata, H. Fukano, H. Nakajima, Y. Akage, and H. Yasaka, "High-performance inp-based

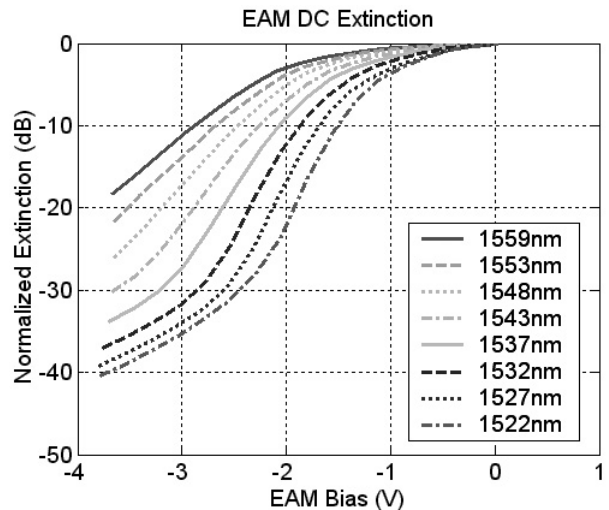


Fig. 7. Normalized DC extinction curves measured over the wavelength tuning range of the SG-DBR laser.

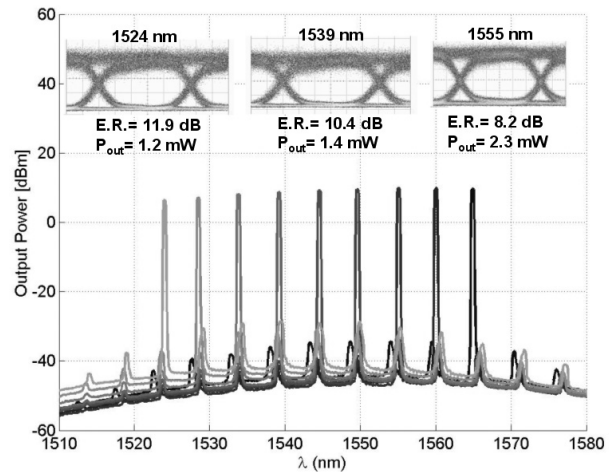


Fig. 8. Overlaid optical spectra depicting the supermodes of the widely tunable SG-DBR. Inset: Transmitted eye diagrams at 10 Gbps NRZ. Wavelength, extinction ratio, and optical amplitude are shown.

optical modulators," in *Optical Fiber Communication Conference, 2006 and the 2006 National Fiber Optic Engineers Conference, 2006*, pp. 3 pp.-.

[2] Y.-J. Chiu, T.-H. Wu, W.-C. Cheng, F. Lin, and J. Bowers, "Enhanced performance in traveling-wave electroabsorption modulators based on undercut-etching the active-region," *Photonics Technology Letters, IEEE*, vol. 17, no. 10, pp. 2065–2067, 2005.

[3] R. Lewen, S. Irmscher, U. Westergren, L. Thylen, and U. Eriksson, "Segmented transmission-line electroabsorption modulators," *Lightwave Technology, Journal of*, vol. 22, no. 1, pp. 172–179, 2004.

[4] S. Zhang, V. Kaman, A. Keating, Y.-J. Chiu, P. Abraham, and J. Bowers, "30 gbit/s operation of a traveling-wave electroabsorption modulator," in *Optical Fiber Communication Conference, 1999, and the International Conference on Integrated Optics and Optical Fiber Communication. OFC/IOOC '99. Technical Digest*, vol. 3, 1999, pp. 290–292 vol.3.

[5] G. Li, S. Pappert, P. Mages, C. Sun, W. Chang, and P. Yu, "High-saturation high-speed traveling-wave ingaasp-inp electroabsorption modulator," *Photonics Technology Letters, IEEE*, vol. 13, no. 10, pp. 1076–1078, 2001.

[6] T. Knodl, C. Hanke, B. Saravanan, M. Peschke, R. Macaluso, and B. Stegmuller, "40 GHz monolithic integrated $1.3 \mu\text{m}$ InGaAlAs-InP laser-modulator with double-stack MQW layer structure," in *Lasers and Electro-Optics Society, 2004. LEOS 2004. The 17th Annual Meeting of the IEEE*, vol. 2, 2004, pp. 675–676 Vol.2.

- [7] M. Sysak, J. Raring, J. Barton, M. Dummer, D. Blumenthal, and L. Coldren, "A single regrowth integration platform for photonic circuits incorporating tunable sgdbr lasers and quantum-well eams," *Photonics Technology Letters, IEEE*, vol. 18, no. 15, pp. 1630–1632, 2006.
- [8] R. Spickermann and N. Dagli, "Experimental analysis of millimeter wave coplanar waveguide slow wave structures on gaas," *Microwave Theory and Techniques, IEEE Transactions on*, vol. 42, no. 10, pp. 1918–1924, 1994.
- [9] R. Lewen, S. Irmscher, and U. Eriksson, "Microwave cad circuit modeling of a traveling-wave electroabsorption modulator," *Microwave Theory and Techniques, IEEE Transactions on*, vol. 51, no. 4, pp. 1117–1128, 2003.